A Misalignment-Tolerant Fractional-Order Wireless Charging System With Constant Current or Voltage Output

Chao Rong, Bo Zhang, *Senior Member, IEEE*, Yanwei Jiang, Xujian Shu, and Zhihao Wei

***Abstract*—Wireless charging of automated guided vehicles (AGVs) has been widely used because of its high security and convenience. However, due to the inevitable misalignment between the coupling coils, the charging system cannot maintain the constant current (CC) or constant voltage (CV) output. Therefore, this article proposes a misalignment-tolerant fractional-order wireless power transfer (FOWPT) system with CC or CV output. According to the principle of the fractional-order autonomous circuit, the natural resonant frequency and operating frequency can be adjusted adaptively with the change of transfer distance and load. Benefiting from the frequency characteristics and the new implementation method of the FOWPT, the system maintains CC and CV output, and the horizontal and vertical misalignment tolerances are within 44.4% and 22.2%, respectively. Therefore, the proposed system improves the freedom and convenience of charging, and provides a new wireless charging solution for AGVs. Future article will focus on more concise modeling and implementation methods of fractional-order systems, and improving the performance of the FOWPT.**

***Index Terms*—Autonomous circuit, constant current (CC)/voltage charging, fractional order, wireless power transfer (WPT).**

NOMENCLATURE

ω	Operating frequency.
$\omega_1(\omega_2)$	Primary (secondary) natural resonant frequency.
$C_{\alpha1}(C_{\alpha2})$	Primary (secondary) pseudocapacitance.
$C_{e1}(C_{e2})$	Fractional equivalent capacitance of $C_{\alpha1}(C_{\alpha2})$.
$\alpha_1(\alpha_2)$	Fractional order of $C_{\alpha1}(C_{\alpha2})$.
α_C	Critical fractional order.
$L_{\beta1}(L_{\beta2})$	Primary (secondary) pseudoinductance.
$L_{e1}(L_{e2})$	Fractional equivalent inductance of $L_{\beta1}(L_{\beta2})$.
$\beta_1(\beta_2)$	Fractional order of $L_{\beta1}(L_{\beta2})$.
M	Mutual inductance of the magnetic coupler.
k	Coupling strength of the magnetic coupler.
k_C	Critical coupling strength k_C.
$R_{C\alpha1}(R_{C\alpha2})$	Equivalent resistance of $C_{\alpha1}(C_{\alpha2})$.
$R_{L\beta1}(R_{L\beta2})$	Equivalent resistance of $L_{\beta1}(L_{\beta2})$.
$R_1(R_2)$	Primary (secondary) internal resistance.
R_B	Equivalent load resistance of the battery.
R_L	Equivalent ac resistance of the rectifier.
$X_{C\alpha1}(X_{C\alpha2})$	Equivalent reactance of $C_{\alpha1}(C_{\alpha2})$.
$X_{L\beta1}(X_{L\beta2})$	Equivalent reactance of $L_{\beta1}(L_{\beta2})$.
X_M	Equivalent reactance of M.
D	Vertical distance.
ρ	Horizontal offset distance.
V_d	Input dc voltage.
$V_{B\mathrm{ref}}$	Constant charging voltage.
$I_{B\mathrm{ref}}$	Constant charging current.
P_o	Output power.
η	Transfer efficiency.
η_D	dc–dc efficiency.

Manuscript received December 14, 2021; revised February 27, 2022; accepted March 28, 2022. Date of publication April 1, 2022; date of current version May 23, 2022. This work was supported by the Key Program of National Natural Science Foundation of China under Grant 51437005. Recommended for publication by Associate Editor M. Vitelli. *(Corresponding author: Bo Zhang.)*

Chao Rong, Bo Zhang, Xujian Shu, and Zhihao Wei are with the School of Electric Power, South China University of Technology, Guangzhou 510640, China (e-mail: eprongchao@mail.scut.edu.cn; epbzhang@scut.edu.cn; epshuxujian@163.com; hankwei0722@163.com).

Yanwei Jiang is with the College of Electrical Engineering and Automation, Fuzhou University, Fuzhou 350000, China (e-mail: jiang_yanwei@foxmail.com).

Color versions of one or more figures in this article are available at https://doi.org/10.1109/TPEL.2022.3164069.

Digital Object Identifier 10.1109/TPEL.2022.3164069

I. INTRODUCTION

WITH the development of technology, automated guided vehicle (AGV) has been applied in many fields [1]–[3]. Here, the battery stores and provides energy for the system. The safety and effectiveness of its charging system are important to the entire system. Compared with conventional wired charging solutions, wireless power transfer (WPT) has higher reliability, safety, and convenience, which can be applied in some extreme environments and special conditions [4]. Therefore, WPT is expected to become the most popular charging solution for AGV. In order to improve the safety and service life of the battery, constant current (CC) and constant voltage (CV) charging is a typical charging solution [5]. This requires the WPT system to keep CC or CV unchanged when the equivalent resistance of the battery changes. In addition, the transfer distance is not constant due to the inevitable misalignment. In order to greatly improve the freedom and applicability of wireless charging, it is also crucial to improve the misalignment tolerance of the WPT system.

A number of new solutions has been proposed to achieve CC and CV charging within a certain range, which can be classified into inherent properties of geometry and closed-loop control solutions. The geometry includes the structure of the coupled

coils and the compensation topology. The magnetic field can be uniformly distributed to improve the misalignment tolerance by designing special coil structures, including DD [6], tri-polar [7], array coils [8], and three-dimensional coils [9]. Although the change of mutual inductance is greatly reduced, the mutual inductance is still not strictly constant. Therefore, in the application of wireless charging for AGV, the output accuracy of CC and CV modes will be difficult to guarantee. In addition, high-order compensation topology such as *LCC* compensation is another popular method [10]. By constructing high-order compensation with CC or CV output, load-independent WPT systems can be realized. In addition, load-independent wireless charging can also be realized by switching the compensation topology [11], [12]. Benefiting from the special coil design and the reconfigurable resonant circuit, the system can be flexibly switched between CC and CV modes [12]. Meanwhile, by setting the position of the relay coil, the desired values of output voltage and current can be adjusted. This solution avoids complex control strategies. However, CC or CV cannot be guaranteed when the receiver moves during charging. The stability and security need strict analysis and design because of the transient process caused by the switching of compensation topology. With the development of WPT, the combination of special coil structure and hybrid compensation topology to achieve high misalignment tolerance is also a good solution [13]. However, these solutions face common problems such as large size, high cost, and low output accuracy.

The closed-loop control solutions mainly include the additional dc–dc converter, phase-shift control, and frequency tracking technology. These solutions generally require load information, which can be obtained by wireless communication or parameter identification technology. With the help of wireless communication channels, the simultaneous wireless power and data transfer system can still maintain a stable output when the transfer distance and load change [14]. However, there is interference between the energy and data channel in practical applications due to the inevitable coupling between coils. When the transfer distance and the load continuously change, it will reduce the data transfer stability and increase the bit error rate. This may lead to the failure of dynamic charging. Meanwhile, it is also not suitable for compact and lightweight receivers. Another method is load identification [15], [16], which can be based on the reflected impedance, frequency scanning, switching capacitance, etc. This method needs to overcome the errors introduced by the measurement noise and parameter tolerance. Besides, different from the nonautonomous circuit systems with fixed-frequency excitation sources, a PT symmetric WPT system was proposed [17]. By constructing an inductive power transfer (IPT) system that satisfies the PT symmetry, the system realizes constant power in the PT-symmetry region. Although this system requires a strict symmetry relationship of circuit parameters and is very sensitive to the natural resonant frequency, it shows another perspective on the WPT.

Therefore, exploring new mechanisms and perspectives of WPT is a way to achieve the high misalignment-tolerant WPT system. It is well known that the integer-order WPT system has received much attention and research. However, more and more studies have focused on fractional-order systems, which exhibit interesting characteristics [18]. In fact, the concept of fractional calculus (FC) has been proposed almost simultaneously with classical calculus. FC can go back to Leibniz's letter in 1695 [19]. Due to the lack of background disciplines such as physics, FC has been in pure mathematics for a long time. Until 1823, Abel first applied FC to solve the integral equation of the isochronous curve. Since then, FC provides an excellent theory in many areas of research and has demonstrated the incomparable advantages of integer-order systems in terms of modeling and control [20]. For three centuries, the definitions of FC were proposed by Liouville *et al.* [21]. Recently, the Riemann–Liouville definition is the most widely known definition of the fractional derivative, which is expressed as

$$ {}_aD_t^v f(t) = \frac{1}{\Gamma(n-v)} \frac{d^n}{dt^n} \int_a^t \frac{f(\tau)}{(t-\tau)^{v+1-n}} d\tau, n-1 \le v < n \tag{1} $$

where ${}_aD_t^v$ is equal to d^v/dt^v, a is the initial time, n is an integer, v is the order of the derivative, and $\Gamma(x)$ is the Gamma function. In the zero-initial state, the Laplace transform of (1) can be expressed as $D^v f(t) \Leftrightarrow s^v F(s)$.

Applying FC, many new characteristics have been discovered in the field of electronic circuits. It has been found that the resonant frequency and impedance characteristics of fractional-order LC circuits are different under different fractional orders [22]. Then, benefiting from FC, a fractional-order wireless power transfer (FOWPT) system was proposed, which employs fractional-order capacitors (FOC) and fractional-order inductors (FOI) [23]. Generally, FOWPT systems can be divided into nonautonomous fractional-order systems with fixed-frequency excitation sources and autonomous fractional-order systems powered by fractional-order elements. Benefiting from the implementation of fixed-frequency FOC [24], a nonautonomous FOWPT system can realize load-independent CC output at a fixed distance [25]. In terms of modeling of FOWPT, the approximation method of coupled modes is mainly used to simplify the analysis. Based on FC and the coupled mode theory, a generalized fractional coupled model was proposed in [26]. The dynamic characteristic of FOWPT was analyzed for the first time, which revealed the difference in dynamic response between fractional-order and integer-order systems. However, the proposed model is complicated and difficult to solve the generalized fractional-order coupled-mode equations, which cannot be used in closed-loop control. In order to make the model greatly simplified, an approximate coupled model based on the Taylor series method was proposed in [27]. Under the approximate conditions of weak coupling and high-quality factors, the Taylor series method is used to simplify the model of the system. Since the model is limited by the above constraints, the accuracy of the output characteristics and critical working region obtained by this coupled model cannot be guaranteed. Therefore, this model is limited in practical applications, especially in CC or CV wireless charging. It is impossible to accurately realize the output of CC or CV by primary-side-only control. Besides, the accuracy of the fractional order and the realization of soft switching need to be further studied.

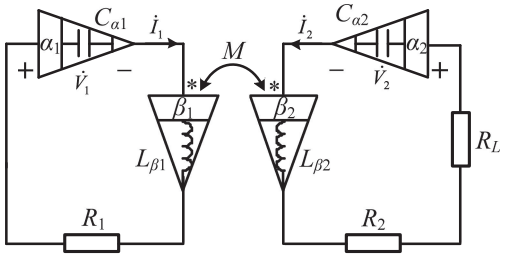

Fig. 1. Simplified circuit diagram of the FOWPT.

It can be seen that the setting of approximate conditions brings more inaccuracy. Meanwhile, those approximation conditions also prevent some peculiar characteristics from being discovered. On the other hand, high-precision fractional-order elements need to be solved urgently. Therefore, the FOWPT with application potential deserves more in-depth research. The main motivation of this article is to propose a novel misalignment-tolerant FOWPT system and its model and control strategy. The main contributions are as follows:

1) A general FOWPT system is proposed, which is an autonomous system. An accurate model of the FOWPT system is obtained, and frequency characteristics are analyzed in detail.
2) Benefiting from the frequency characteristics of autonomous fractional-order system, CC and CV output are realized by primary-side-only control. The system has high misalignment tolerance and good dynamic performance.
3) An innovative implementation method of active FOC based on the phase-shift control is proposed, which not only greatly improves the accuracy and responsiveness of FOC, but also realizes zero-voltage switching (ZVS).
4) By flexibly adjusting the fractional order, this system can be applied to different types of receivers, and the charging region can also be designed.

Knowing these descriptions in mind, this article is organized as follows. Section II analyzes a general FOWPT system based on the autonomous circuit theory. The frequency characteristics and system performance of the FOWPT system are given in Section III. Subsequently, a wireless CC/CV charging system of AGV based on FOWPT is established in Section IV. Finally, Section V draws some important conclusions.

II. System Structure and Principle

A. System Structure of FOWPT

Fig. 1 represents a schematic diagram of an FOWPT system, which is different from the classic integer-order WPT system. In general, an FOWPT system consists of a transmitter, receiver, and load. The transmitter and receiver achieve WPT by mutual inductance M. The energy of the load is provided by the fractional elements instead of fixed frequency excitation source. The meanings of the symbols are in the nomenclature, which is adopted throughout this article.

The transmitter comprises a primary-side $L_{\beta 1}$, a primary-side FOC $C_{\alpha 1}$, and an internal resistance R_1 that are connected in series. The receiver comprises a secondary-side FOI $L_{\beta 2}$, a secondary-side FOC $C_{\alpha 2}$, an internal resistance R_2, and load R_L that are connected in series. In addition, β_1 and β_2 are the order of the primary-side and secondary-side FOI, respectively; $L_{\beta 1}$ and $L_{\beta 2}$ are the pseudoinductance of the primary-side and secondary-side FOI, respectively; α_1 and α_2 are the order of the primary-side and secondary-side FOC, respectively; and $C_{\alpha 1}$ and $C_{\alpha 2}$ are the pseudocapacitance of the primary-side and secondary-side FOC, respectively. It should be noted that if all fractional orders are one, the FC will be the traditional integer calculus according to (1). Meanwhile, the fractional-order elements in FOWPT system will become conventional integer-order capacitors and inductors. In this case, the system is an integer-order WPT system, obviously. It can be found that the FOWPT system is a general description of the integer-order WPT system, that is, the integer-order WPT is a special case. Therefore, FOWPT has higher design freedom and more valuable characteristics.

B. Condition for Steady State

According to the circuit theory [28], the volt–ampere characteristic equations of FOI and FOC are defined as

$$\begin{cases} v_{Ln}(t) = L_{\beta n}\frac{d^{\beta_n} i_{Ln}(t)}{dt^{\beta_n}} \\ i_{Cn}(t) = C_{\alpha n}\frac{d^{\alpha_n} v_{Cn}(t)}{dt^{\alpha_n}} \end{cases}, n = 1, 2 \tag{2}$$

where the subscript 1 (or 2) refers to the transmitter (or receiver); $d^{\beta n}/dt^{\beta n}$ and $d^{\alpha n}/dt^{\alpha n}$ are termed as the fractional-order derivative; $i_{Ln}(t)$ and $i_{Cn}(t)$ are the current of FOI and FOC, respectively; $v_{Ln}(t)$ and $v_{Cn}(t)$ are the voltage of FOI and FOC, respectively; $L_{\beta n}$ and $C_{\alpha n}$ are the inductance with its unit H/s$^{1-\beta n}$ and the capacitance with its unit F/s$^{1-\alpha n}$, respectively; and α_n and β_n are the order of FOI and FOC, respectively. If α_n and β_n are one, the volt–ampere characteristic equations will be equivalent to those of conventional capacitors and inductors.

For $s = j\omega$, (2) can be written in the form of frequency domain with zero initial condition as $Z_{Cn} = [\cos(\alpha_n\pi/2) - j\sin(\alpha_n\pi/2)]/\omega^{\alpha n}C_{\alpha n}$, and $Z_{Ln} = \omega^{\beta n}L_{\beta n}[\cos(\beta_n\pi/2) + j\sin(\beta_n\pi/2)]$. It indicates that the impedance of the FOI and FOC can be expressed as the sum of a reactance component and a resistance component. Therefore, the fractional equivalent capacitance is $C_{en} = \omega^{\alpha\text{-}1}C_\alpha/\sin(\alpha\pi/2)$, and the fractional equivalent inductance is $L_{en} = \omega^{\beta\text{-}1}L_\beta/\sin(\beta\pi/2)$. Then, the resonant frequency ω_{rn} can be expressed as $[\sin(\alpha_n\pi/2)/L_{\beta n}C_{\alpha n}\sin(\beta_n\pi/2)]^{1/(\alpha n + \beta n)}$.

On the basis of Kirchhoff's voltage and current laws, the FOWPT system in Fig. 1 can be fully described by phasor equations as follows:

$$\begin{cases} 0 = \dot{V}_1 + (j\omega)^{\beta_1}L_{\beta_1}\dot{I}_1 + j\omega M\dot{I}_2 + R_1\dot{I}_1 \\ \dot{I}_1 = (j\omega)^{\alpha_1}C_{\alpha_1}\dot{V}_1 \\ 0 = \dot{V}_2 + j\omega M\dot{I}_1 + (j\omega)^{\beta_2}L_{\beta_2}\dot{I}_2 + (R_2 + R_L)\dot{I}_2 \\ \dot{I}_2 = (j\omega)^{\alpha_2}C_{\alpha_2}\dot{V}_2. \end{cases} \tag{3}$$

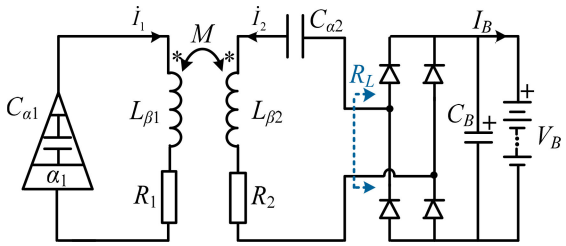

Fig. 2. Circuit diagram of the FOWPT system with an active FOC.

In order to obtain the current distribution, (3) can be further simplified as

$$\begin{cases} 0 = \left[R_{e1} + j\left(X_{L_{\beta 1}} - X_{C_{\alpha 1}}\right)\right]\dot{I}_1 + jX_M\dot{I}_2 \\ 0 = jX_M\dot{I}_1 + \left[R_{e2} + j\left(X_{L_{\beta 2}} - X_{C_{\alpha 2}}\right)\right]\dot{I}_2 \end{cases} \tag{4}$$

where $R_{e1} = R_1 + R_{L\beta 1} + R_{C\alpha 1}$ and $R_{e2} = R_2 + R_{L\beta 2} + R_{C\alpha 2} + R_L$ are equivalent total resistances of the transmitter and receiver, respectively; $R_{L\beta n} = \omega^{\beta n} L_{\beta n}\cos(\beta_n\pi/2)$ is equivalent resistance of FOI; $R_{C\alpha n} = \cos(\alpha_n\pi/2)/\omega^{\alpha n}C_{\alpha n}$ is equivalent resistance of FOC; $X_{L\beta n} = \omega^{\beta n}L_{\beta n}\sin(\beta_n\pi/2)$ is equivalent reactance of FOI; and $X_{C\alpha n} = \sin(\alpha_n\pi/2)/\omega^{\alpha n}C_{\alpha n}$ is equivalent reactance of FOC ($n = 1, 2$). $X_M = \omega M$ is equivalent reactance of M. It is worth noting that $R_{L\beta n}$ and $R_{C\alpha n}$ will be negative when the corresponding fractional order is set to be greater than one. In this case, the fractional-order element is an active element and can provide energy for the load. In addition, the reactance in FOWPT system is related not only to the value and frequency of capacitance or inductance, but also to the fractional order. This characteristic improves the design freedom of fractional-order systems.

When the determinant of the matrix coefficients is equal to zero, (4) has nonzero solutions. Then, by separating the real and imaginary parts, the characteristic equation of this system can be obtained as

$$\begin{cases} R_{e1}R_{e2} - \left(X_{L_{\beta 1}} - X_{C_{\alpha 1}}\right)\left(X_{L_{\beta 2}} - X_{C_{\alpha 2}}\right) + X_M^2 = 0 \\ R_{e1}\left(X_{L_{\beta 2}} - X_{C_{\alpha 2}}\right) + R_{e2}\left(X_{L_{\beta 1}} - X_{C_{\alpha 1}}\right) = 0. \end{cases} \tag{5}$$

It is obvious that if all orders are one, (5) will become the integer-order equations of conventional WPT.

III. Theoretical Analysis and System Design

A. Theoretical Analysis

According to the unique characteristics of FOWPT mentioned in Section II, an FOWPT system for CC or voltage output is designed, as shown in Fig. 2. In order to obtain the simplest fractional topology and compact receiver, an active FOC is employed to provide energy for the load, that is, the fractional order $\alpha_1 > 1$ and $\alpha_2 = \beta_1 = \beta_2 = 1$. Using one active fractional-order element is the simplest way to implement a fractional-order wireless charger.

For the full-bridge rectifier in Fig. 2, the relationship between the charging current I_B and root-mean-square (rms) value of $\dot{I}_2$ can be expressed as

$$I_B = \frac{1}{\pi}\int_0^{\pi}\sqrt{2}I_2\sin(\omega t)\,d(\omega t) = \frac{2\sqrt{2}}{\pi}I_2. \tag{6}$$

When the power losses of the rectifier bridge are ignored, we can obtain $I_2^2R_L = I_B^2R_B$ based on the law of conservation of energy. It is noted that R_B is the equivalent load resistance of battery. Then, the equivalent load R_L of the rectifier is deduced as $R_L = 8R_B/\pi^2$. Knowing the above analysis in mind, the characteristics of the natural resonant frequency ω_1 and operating frequency ω will be analyzed in this section. Then, the current distribution $|\dot{I}_1/\dot{I}_2|$ and CC/CV mode will be studied, which are completely different from the classical integer-order WPT in some aspects.

Knowing (5), the characteristic equation of the FOWPT system in Fig. 2 is given by

$$\begin{cases} \left(R_1 + R_{C_{\alpha 1}}\right)\left(R_2 + R_L\right) \\ -\left(X_{L_{\beta 1}} - X_{C_{\alpha 1}}\right)\left(X_{L_{\beta 2}} - X_{C_{\alpha 2}}\right) + X_M^2 = 0 \\ \left(R_1 + R_{C_{\alpha 1}}\right)\left(X_{L_{\beta 2}} - X_{C_{\alpha 2}}\right) \\ +\left(R_2 + R_L\right)\left(X_{L_{\beta 1}} - X_{C_{\alpha 1}}\right) = 0. \end{cases} \tag{7}$$

Then, (7) can be expanded as follows:

$$\begin{cases} \left(\frac{R_1}{\omega L_{\beta_1}} + \frac{\omega_1^{\alpha_1+1}}{\omega^{\alpha_1+1}}\cot\frac{\alpha_1\pi}{2}\right)\frac{(R_2+R_L)}{\omega L_{\beta_2}} \\ -\left(1 - \frac{\omega_1^{\alpha_1+1}}{\omega^{\alpha_1+1}}\right)\left(1 - \frac{\omega_2^2}{\omega^2}\right) + k^2 = 0 \\ \left(\frac{R_1}{\omega L_{\beta_1}} + \frac{\omega_1^{\alpha_1+1}}{\omega^{\alpha_1+1}}\cot\frac{\alpha_1\pi}{2}\right)\left(\omega - \frac{\omega_2^2}{\omega}\right) \\ +\frac{(R_2+R_L)}{L_{\beta_2}}\left(1 - \frac{\omega_1^{\alpha_1+1}}{\omega^{\alpha_1+1}}\right) = 0 \end{cases} \tag{8}$$

where ω_1 and ω_2 are natural resonant frequencies of the transmitter and receiver, respectively; and $k = M/\sqrt{L_{\beta_1}L_{\beta_2}}$ denotes the mutual coupling strength. From (8), the natural resonant frequency ω_1 of the transmitter can be expressed as

$$\omega_1 = \omega\left\{\frac{R_1\left(\omega - \frac{\omega_2^2}{\omega}\right)\Big/\omega L_{\beta_1} + (R_2 + R_L)/L_{\beta_2}}{\left[(R_2 + R_L)/L_{\beta_2} - \left(\omega - \frac{\omega_2^2}{\omega}\right)\cot(\alpha_1\pi/2)\right]}\right\}^{\frac{1}{1+\alpha_1}}. \tag{9}$$

Substituting (9) into (8), the frequency polynomial equation can be derived as

$$\begin{aligned} &\left(1 - k^2\right)\omega^5 + \left(\Gamma_{10} + \Gamma_{2L}k^2\right)\tan\frac{\alpha_1\pi}{2}\omega^4 \\ &\quad + \left[\Gamma_{2L}^2 + \left(k^2 - 2\right)\omega_2^2\right]\omega^3 + \left(\Gamma_{2L}^2 - 2\omega_2^2\right)\Gamma_{10} \\ &\quad \times \tan\frac{\alpha_1\pi}{2}\omega^2 + \left(\omega_2^4\right)\omega + \Gamma_{10}\tan\frac{\alpha_1\pi}{2}\omega_2^4 = 0 \end{aligned} \tag{10}$$

where $\Gamma_{10} = R_1/L_{\beta 1}$ and $\Gamma_{20} = R_2/L_{\beta 2}$ are defined as the intrinsic loss rate of the transmitter and receiver, respectively; and $\Gamma_L = R_L/L_{\beta 2}$ is the loss rate contributed by the load and the total loss rate can be expressed as $\Gamma_{2L} = \Gamma_{20} + \Gamma_L$. Since FOWPT is an autonomous system without fixed-frequency forced excitation source, the operating frequency is determined by (11), and its analytical solution needs to be analyzed first [29]. Meanwhile, quality factor of the transmitter ($Q_{10} = \omega_2/\Gamma_{10}$) and

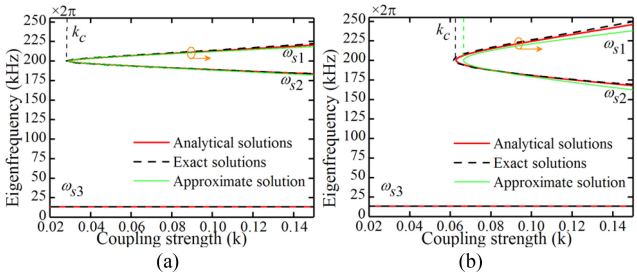

Fig. 3. Eigenfrequency as a function of coupling strength k. (a) $R_L = 5\ \Omega$. (b) $R_L = 25\ \Omega$.

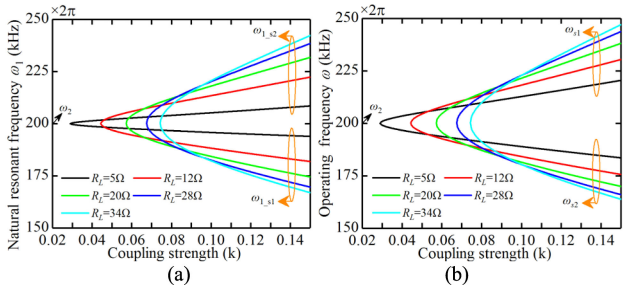

Fig. 4. Natural resonant frequency ω_1 and operating frequency ω as a function of coupling strength k when $R_L = \{5, 12, 20, 28, 34\}$. (a) Natural resonant frequency ω_1. (b) Operating frequency f.

receiver ($Q_{2\mathrm{L}} = \omega_2/\Gamma_{2\mathrm{L}}$) are high. In the case of finite fractional order, coupling strength and load resistance, $k^2\tan(\alpha_1\pi/2)/Q_{10}$ and $k^2\tan^2(\alpha_1\pi/2)(1/Q_{10} + 1/Q_{2\mathrm{L}})/Q_{10}$ are high-order small quantities, which can be approximated and ignored. Then, by factorization, the frequency polynomial equation (10) can be expressed as

$$\left(\omega + \Gamma_{10}\tan\frac{\alpha_1\pi}{2}\right)\left\{\left(1-k^2\right)\omega^4 + \xi\omega^2 + \omega_2^4\right\} = 0 \quad (11)$$

where $\xi = \Gamma_{2L}^2 + (k^2-2)\omega_2^2 + k^2\omega_2(\Gamma_{10}+\Gamma_{2L})\tan\alpha_1\pi/2$. According to (11), three eigenfrequencies are derived as

$$\begin{cases} \omega_{s1,s2} = \sqrt{\left[-\xi \pm \sqrt{\xi^2 - 4\left(1-k^2\right)\omega_2^4}\right] \Big/ 2\left(1-k^2\right)} \\ \omega_{s3} = -\Gamma_{10}\tan\left(\alpha_1\pi/2\right). \end{cases} \quad (12)$$

Equation (12) indicates that the FOWPT system has two different working regions, which are determined by the critical coupling strength k_C in (13). In the strongly coupled region ($k > k_C$), the two resonators have three stable operating frequencies (ω_{s1}, ω_{s2}, or ω_{s3}). In the weak coupling region ($k < k_C$), the system enters a single frequency (ω_{s3}) working region

$$k_C = \sqrt{\frac{2\sigma Q_{2L}^2 + \sqrt{4\sigma^2 Q_{2L}^4 - (1+\sigma)^2\left(1-4Q_{2L}^2\right)}}{(1+\sigma)^2 Q_{2L}^2}} \quad (13)$$

where $\sigma = (1/Q_{10} + 1/Q_{2L})\tan(\alpha_1\pi/2)$. Meanwhile, for a certain transfer distance, there is a critical fractional order for the fractional-order system as shown in (14)

$$\alpha_C = \frac{2}{\pi}\arctan\left\{\frac{Q_{10}Q_{2L}}{Q_{10}+Q_{2L}} \times \left[\frac{2}{k^2} - 1 - \sqrt{\frac{4}{k^4} - \frac{4}{k^2} - \frac{1}{k^4 Q_{2L}^2}\left(\frac{1}{Q_{2L}^2} - 4\right)}\right]\right\}. \quad (14)$$

In other words, a desired charging region can be obtained by adjusting the fraction order. The high design freedom of fractional-order system is fully revealed.

Fig. 3 gives three eigenfrequencies. With the increase of load resistance and transfer distance, the approximate solution obtained by [27] and its critical coupling coefficient k_c have large errors. There is a good agreement between the analytical solutions obtained by (12) in this article and exact solutions obtained by (10). In addition, it can be found that the region can be divided into two parts. In the fractional working region ($k > k_C$), there are three eigenvalues. Beyond this region, the system will automatically operate at ultra-low frequency solution ω_{s3} and the corresponding output power is extremely low. Therefore, it can effectively avoid overcurrent when the receiver is beyond the charging region.

From (9) and (12), it can be seen that the natural resonant frequency (ω_1) and operating frequency (ω) of the transmitter in FOWPT systems will change under different transfer distances and loads. Furthermore, combined with (8), the coupling strength k and load R_L can be obtained as

$$k = \sqrt{\left(1 - \frac{\omega_2^2}{\omega^2}\right)\left[(1-\delta) + \left(\frac{R_1}{\omega L_{\beta_1}} + \delta\cot\frac{\alpha_1\pi}{2}\right)^2 \Big/ (1-\delta)\right]} \quad (15)$$

$$R_L = \left(\frac{L_{\beta_2}R_1}{L_{\beta_1}} + \omega L_{\beta_2}\delta\cot\frac{\alpha_1\pi}{2}\right)\left(\frac{\omega_2^2}{\omega^2} - 1\right)\Big/(1-\delta) - R_2 \quad (16)$$

where $\delta = \omega\alpha_1 + 11/\omega^{\alpha 1+1}$. It should be noted that an FOWPT system powered by FOC is an autonomous circuit system. Benefiting from the unique frequency characteristics of the FOC, ω_1 and ω can be adjusted automatically. Therefore, using (15) and (16), the coupling strength k and load R_L can be calculated in real time.

In order to analyze the energy transfer process, current distribution and output power are concerned. According to (4) and (8), the current distribution can be derived as

$$K_i = \left|\frac{\dot{I}_1}{\dot{I}_2}\right| = \sqrt{-\frac{(R_2+R_L)\tan\left(\alpha_1\pi/2\right)}{R_1\tan\left(\alpha_1\pi/2\right) + \omega_1^{1+\alpha_1}L_{\beta_1}/\omega^{\alpha_1}}} \quad (17)$$

where the natural resonance frequency ω_1 and operating frequency ω automatically adjust with the change of distance according to (9) and (12). It can be found from Fig. 4 that the changing trends of ω_1 and ω are the same, which greatly reduces the change of circuit distribution. With the increase of distance, $\omega\alpha_1 + 11/\omega^{\alpha 1}$ will approach ω_2 under a fixed fractional order α_1 and load R_L. Meanwhile, K_i will also approach a constant ratio, which makes the output power and transfer efficiency insensitive to the change of transfer distance. Considering the current distribution (17), the transfer efficiency η can be

TABLE I
CONFIGURATION OF THE FOWPT SYSTEM

Parameter	Value	Parameter	Value
R_1	133.5 mΩ	R_2	252.5 mΩ
α_1	1.015	$C_{\alpha 2}$	5.361nF
$L_{\beta 1}$	67.6μH	$L_{\beta 2}$	115.97μH
D	6-8 cm	ρ	0-4 cm
V_d	65 V	R_B	5-7Ω (CC)
$\omega_2/2\pi$	201.8 kHz		7-42Ω(CV)

derived as

$$\eta = \frac{P_o}{P_{in}} = \frac{I_2^2 R_L}{I_1^2 R_1 + I_2^2 (R_2 + R_L)} = \frac{\frac{\omega^{\alpha_1}}{\omega_1^{1+\alpha_1}} R_1 R_L \tan\frac{\alpha_1 \pi}{2} + R_L L_{\beta_1}}{L_{\beta_1}(R_2 + R_L)}. \quad (18)$$

Generally, the output power is determined by the current distribution in the transmitter and receiver. As K_i approaches the constant value, the efficiency will remain constant. Then, the output power can also be obtained

$$P_o = |I_2|^2 R_L = -\frac{R_1 \tan(\alpha_1 \pi/2) + \omega_1^{1+\alpha_1} L_{\beta_1}/\omega^{\alpha_1}}{(R_2 + R_L)\tan(\alpha_1 \pi/2)} |I_1|^2 R_L \quad (19)$$

where I_1 is rms values of current. By controlling the current of FOC, the output power can be adjusted.

B. Characteristics of the FOWPT System

From the theoretical analysis, it can be seen that the FOWPT system has better performance and greater design freedom due to the application of fractional elements. The following will analyze the frequency characteristics and how to realize the CC and CV modes. The parameter configuration of simulation and experiment is shown in Table I.

According to (12), there are three eigenvalues in the working region ($k > k_C$). According to (9) and (12), the natural resonant frequency ω_1 and operating frequency ω can be adjusted automatically, which are determined by coupling strength k and load R_L, as shown in Fig. 4. Therefore, the natural resonance frequency of the transmitter can be different from that of the receiver. For receivers with different natural resonance frequencies, FOC can also flexibly configure the fractional order to realize efficient power transfer. In addition, the output voltage V_1, current I_1, and operating frequency ω of the FOC satisfy the relationship $\omega_1^{\alpha 1+1} = \omega^{\alpha 1} V_1 \sin(\alpha_1 \pi/2)/L_{\beta 1} I_1$.

The relationship between the order α_1 of the FOC and the critical coupling strength k_C is shown in Fig. 5. When the order α_1 is closer to one, k_C is smaller, that is, the working region is wider. Therefore, the appropriate order can be selected when designing the FOWPT system. Under the parameters in Table I, α_1 is set to 1.015 to meet the requirements of the working range and load. Moreover, the colored arrows mark the corresponding critical transfer distance of integer-order PT-symmetric WPT.

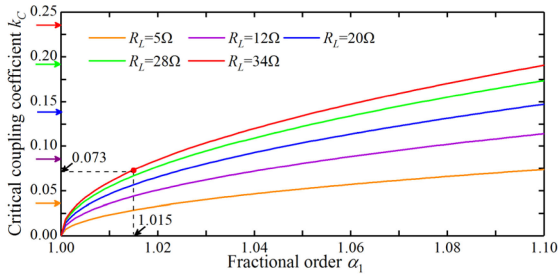

Fig. 5. Critical coupling strength k_C as a function of the fractional order α_1 when $R_L = \{5, 12, 20, 28, 34\}$.

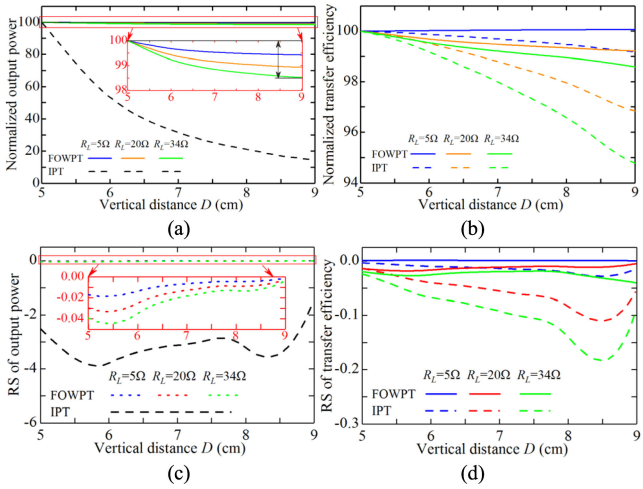

Fig. 6. Sensitivity curves for output power and transfer efficiency. Normalized (a) output power and (b) transfer efficiency as a function of the vertical distance D when $R_L = \{5, 20, 34\}$; RS of (c) output power and (d) transfer efficiency at different vertical distances.

Obviously, the working region of FOWPT has been greatly expanded and can be flexibly adjusted.

In order to analyze the sensitivity of the FOWPT system to the change of distance, the global and local changes of output power and transfer efficiency will be studied. First, the normalized output power P_o^* and transfer efficiency η^* are defined as

$$\begin{cases} P_o^*(D) = P_o(D)/P_o(D_0) \\ \eta^*(D) = \eta(D)/\eta(D_0) \end{cases} \quad (20)$$

where $P_o(D_0)$ and $\eta_o(D_0)$ are the output power and efficiency at the initial position, respectively. When the receiver moves in the charging region, the change of the system output can be reflected. Then, the relative sensitivity (RS) of output power $S_D^{P_o}$ and transfer efficiency S_D^{η} can be defined as

$$\begin{cases} S_D^{P_o}(D) = \frac{\partial P_o}{P_o} \Big/ \frac{\partial D}{D} \\ S_D^{\eta}(D) = \frac{\partial \eta}{\eta} \Big/ \frac{\partial D}{D} \end{cases} \quad (21)$$

which describe the effect of relative changes in transfer distance on performance. Here, the conventional IPT system with fixed frequency is compared with the FOWPT system. For comparison, the primary current of the IPT system is set constant. Then, Fig. 6 shows sensitivity curves for output power and transfer efficiency, when the vertical distance D changes. For

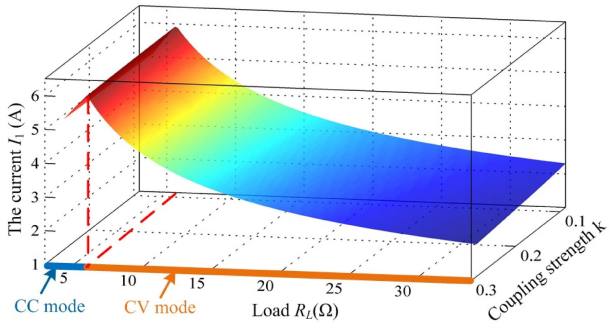

Fig. 7. Three-dimensional graph for the current I_1 of FOC as a function of the coupling strength k and load R_L.

the conventional IPT system, the output power and transfer efficiency vary significantly with distance. For the FOWPT system, the maximum change rate is 1.5%, as shown in Fig. 6(a) and (b). It is precise because of the frequency characteristics of the autonomous FOWPT system that the output power and transfer efficiency remain almost unchanged when D changes. It can also be found from Fig. 6(c) and (d) that the RS of the proposed system is small. It indicates that the current distribution in (17) is also almost unchanged. This is another advantage of the proposed system different from the classical integer-order WPT. In addition, compared to the constant output power and efficiency obtained by the approximate model in [27], the results derived in this article can depict small changes in output power and efficiency. This accurate model provides a theoretical basis for the CC and CV charging of the FOWPT system. And it is worth noting that the corresponding output power and efficiency are almost the same when operating at high frequency (ω_{s1}) and low frequency (ω_{s2}). Since the transfer efficiency corresponding to ω_{s3} is extremely low, the system should avoid running on this frequency.

Moreover, the proposed system can realize wireless charging in the working region by only controlling the output current I_1 of FOC. Considering (6) and (17), when the current I_1 is controlled to $\pi K_i I_{Bref}/2\sqrt{2}$, the system enters the CC mode with CC I_{Bref}. Then, considering (16), the required I_1 is $4K_i V_{Bref}/\sqrt{2}\pi R_L$ in CV mode with CV V_{Bref}. Fig. 7 shows the current I_1 in CC mode and CV mode. It can be seen that the current I_1 is insensitive to the transfer distance. Moreover, considering that the charging process of battery is slow, the equivalent load also changes slowly. Therefore, during the dynamic charging of AGV, the output of FOC only needs to be adjusted slightly, which greatly reduces the requirements for closed-loop systems.

IV. Experiment

It is highly desirable that the wireless charging receiver should not be limited to a specific position. Furthermore, it can be offset or moved within a certain range during charging. Therefore, a misalignment-tolerant wireless charger with CC and CV modes has great theoretical and engineering application value. In this section, a misalignment-tolerant FOWPT system is proposed, which has good dynamic performance and does not need dual-side communication.

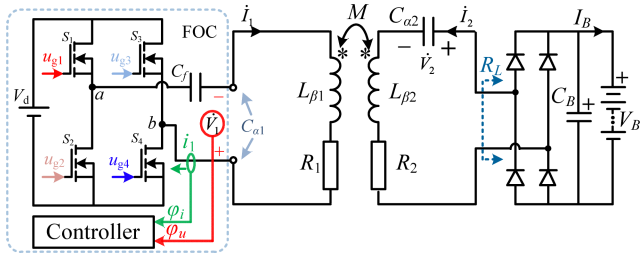

Fig. 8. Circuit diagram of the FOWPT system for CC or CV charging.

A. Design of the FOWPT System

Since it is very difficult to construct high-power and high-stability fractional-order elements, the development of fractional-order wireless charging systems is greatly hampered. The existing construction methods of fractional elements mainly include the following. The first is using inductors and capacitors in series and parallel [21]. The second is based on electrochemical methods, that is, to select electrode surface areas with different dielectric materials [30]. The third is based on silicon process technology, such as using field-effect transistors or CMOS tubes to construct passive FOC with a fixed order [31]. According to the above methods, the fractional-order element constructed can only be passive, which cannot provide energy and the corresponding fractional order is less than one. Besides, the fractional order is unstable under different working conditions. Once the order and operating frequency are changed, it needs to be redesigned and constructed. The fourth is based on the operational amplifier circuit [32], which is limited to low-power applications.

With the rapid development of wide-bandgap semiconductor power devices, the construction of fractional-order elements with any fractional order has attracted more and more attention based on power electronic converters. Based on the phase-locked loop (PLL) and pulsewidth modulation (PWM), the fractional order can be adjusted arbitrarily through digital control, which is suitable for applications with multiple power levels. Fig. 8 gives a circuit diagram of the FOWPT system for CC or CV charging. The main parameters are shown in Table I. By controlling the switching frequency, phase, and duty cycle of full-bridge inverter, a high-power and high-stability FOC is constructed, which provides CC or CV to the battery. It is worth noting that C_f in FOC is used to store electric field energy and participate in filtering.

In order to meet the requirements of fractional-order wireless charging systems, an innovative implementation method of active FOC based on the phase control is proposed. Different from the previous method of actively scanning the frequency and detecting the phase difference between two high-frequency signals in [27], Figs. 8 and 9 show a digital control method that actively controls the phase to maintain the fractional order. Moreover, the proposed method for FOC has the following advantages: 1) there is no need to scan the frequency to reach the fractional order α_1, and dynamic response capability has been greatly improved; 2) it avoids real-time detection of the slight phase difference between two high-frequency signals, which

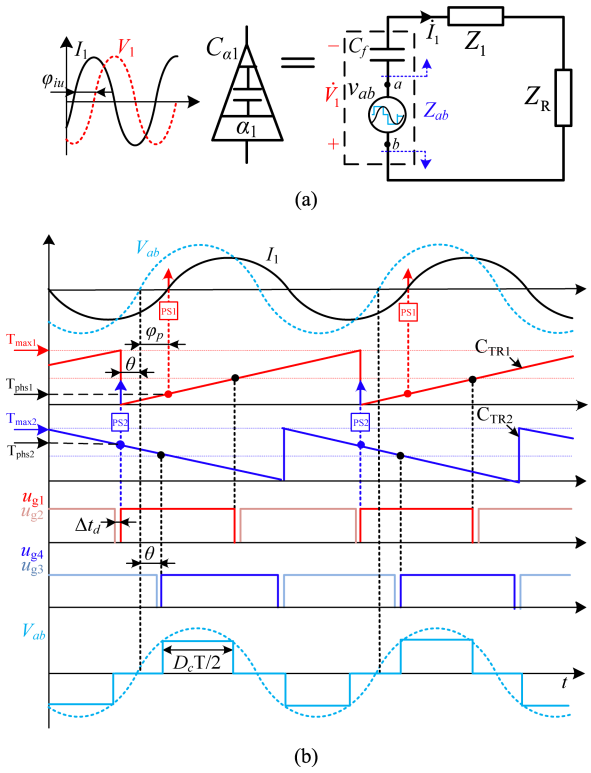

Fig. 9. Implementation strategy of active FOC. (a) Equivalent circuit of FOWPT. (b) Timing diagram of phase control.

improves the accuracy of the order control; and 3) the proposed method realizes soft switching under different distances and loads.

In order to analyze the principle clearly, Fig. 9(a) gives an equivalent circuit diagram. First, the output current I_1 of the FOC generates a square wave through a sampling circuit and zero-crossing comparator. The digital controller obtains the phase and frequency of I_1 by capturing the rising edge [red arrow in Fig. 9(b)] of the square wave. Then, the time-base counters $C_{\mathrm{TR1,2}}$ of two PWM modules are in up-count and down-count mode, respectively. The driving signal u_{g1-4} will flip the level at 0 and $0.5{*}T_{\mathrm{max1,2}}$. In the actual circuit system, the second comparison value will be slightly less than $0.5{*}T_{\mathrm{max1,2}}$, which reserves a certain dead time to discharge the output capacitance of the switches. Finally, the digital controller generates an output voltage V_{ab}, which leads the phase φ_p of circuit I_1 ($\varphi_p = \varphi_{ab}-\varphi_i$). By controlling the synchronization phase T_{phs1} of the first PWM module, the leading phase φ_p can be changed. In addition, the amplitude of V_{ab} can be adjusted by controlling T_{phs2}, and the corresponding duty cycle $D_c = 1-2\theta/\pi$. On this basis, the proposed FOWPT system will automatically run to the stable frequency determined by the following equation and reach a steady state:

$$\varphi_p = \arg\left(Z_{ab}\right) = \arg\left(1/\mathrm{j}\omega C_f + Z_1 + Z_{\mathrm{R}}\right) \tag{22}$$

where $Z_1 = R_1 + \mathrm{j}\omega L_1$, $Z_{\mathrm{R}} = (\omega M)^2/Z_2$ and $Z_2 = R_2 + R_{\mathrm{L}} + \mathrm{j}(\omega L_2 - 1/\omega C_2)$. According to KCL, the constraint equation is

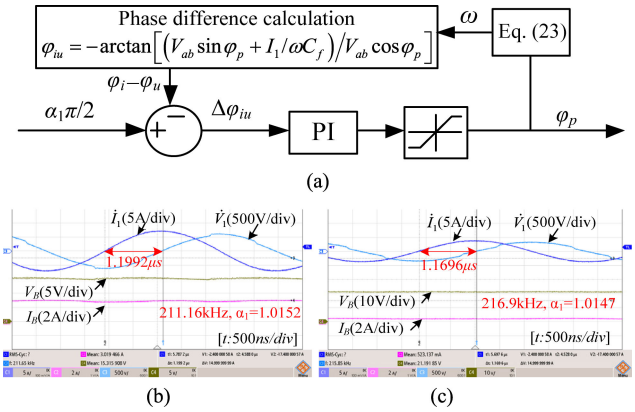

Fig. 10. (a) Phase-locked-loop control to construct an FOC with fractional order α_1. (b) Phase difference and fractional order when $k = 0.096$ and $R_B = 5\ \Omega$. (c) Phase difference and fractional order when $k = 0.089$, $R_B = 40\ \Omega$.

satisfied

$$V_1\angle\varphi_u = -V_{ab}\angle\varphi_{ab} + (I_1/\omega C_f)\angle(\varphi_i - \pi/2) \tag{23}$$

where V_1 and I_1 are rms values of fractional capacitor voltage and current, respectively; the corresponding phases are φ_u and φ_i, respectively; and V_{ab} and φ_{ab} are rms value and phase of the inverter output fundamental voltage, respectively. By separating the real and imaginary parts, the rms value of the output voltage can be expressed as

$$\begin{cases} V_{ab} = -\dfrac{I_1\cos\varphi_{iu}}{\omega C_f\sin(\varphi_{iu}+\varphi_p)} \\ V_1 = -\dfrac{I_1\cos\varphi_p}{\omega C_f\sin(\varphi_{iu}+\varphi_p)}. \end{cases} \tag{24}$$

In order to realize CC and CV mode, a closed-loop control strategy is given in detail in this section. According to the definition of FOC, the phase difference $\varphi_i-\varphi_u$ should be stable at $\alpha_1\pi/2$ to realize the FOC with the order α_1. Fig. 10(a) shows the control strategy of PLL. First, according to the zero-crossing pulse of I_1, control the lead phase φ_p of the first PWM module. Meanwhile, the driving frequency of the PWM module follows the frequency of I_1. Thus, the FOWPT system will automatically run at the frequency ω that satisfies the constraint equation (22). Then, knowing (23) in mind and only by sampling the rms and frequency of I_1, the phase difference $\varphi_i-\varphi_u$ can be calculated by (25). The error of the phase difference is sent to the phase closed-loop controller. Through closed-loop adjustment of φ_p, the order of FOC will eventually stabilize at α_1. It is worth noting that benefiting from the rms sampling chip AD637 and DSP TMS320F28377D, the sampling accuracy can be controlled below 0.05%. Compared with sampling the phase difference between the two high-frequency signals in previous article, the accuracy of the proposed FOC is greatly improved

$$\varphi_i - \varphi_u = -\arctan\left[(V_{ab}\sin\varphi_p + I_1/\omega C_f)/V_{ab}\cos\varphi_p\right] \tag{25}$$

where V_{ab} can be calculated from the duty cycle D_c and satisfies the relationship $V_{ab} = 2\sqrt{2}\sin(0.5D_c\pi)V_{\mathrm{d}}/\pi$. It is worth noting that C_f in FOC not only plays a role in filtering, but also amplifies the phase φ_p compared to $\alpha_1\pi/2$, which greatly mentions the control accuracy of FOC. Fig. 10(b) and (c) shows the phase

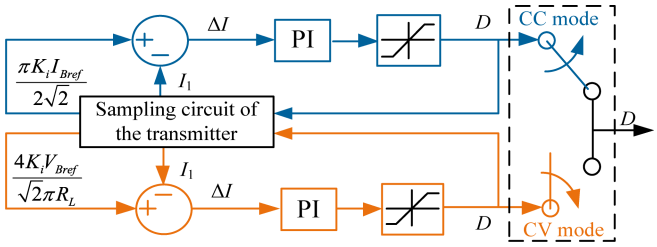

Fig. 11. Control block diagram of CC and CV mode.

difference $\varphi_i - \varphi_u$ and fractional order α_1 of FOC. The fractional order can be controlled at the set value.

Furthermore, since this fractional-order system relies on the active FOC to charge the battery, the FOC should have both CC and CV output capabilities. On the basis of the above principles, Fig. 11 shows the control block diagram of CC and CV mode. By controlling the duty cycle D_c of the inverter, the output voltage V_{ab} can be adjusted in real time. Benefiting from the analysis of Part A in Section III, the FOWPT system can maintain a constant output current I_{Bref} in CC mode and a constant output voltage V_{Bref} in CV mode. Considering (6) and the current ratio K_i given by (17), the output current I_1 of FOC should be controlled as $\pi K_i I_{Bref}/2\sqrt{2}$ and $4K_i V_{Bref}/\sqrt{2}\pi R_L$ in CC mode and CV mode, respectively. In addition, according to (25), the minimum dc voltage V_d needs to be greater than $\pi V_{ab\max}/2\sqrt{2}$ to meet the output requirements.

B. Designing ZVS Switch

In the following part, ZVS conditions will be discussed. According to the above analysis, it can be known that the leading phase φ_p and duty cycle D_c are directly related to the realization of ZVS. When φ_p and α_1 are properly designed, the strategy proposed in Fig. 9 can realize ZVS of all switches. According to (25), φ_p depends on the circuit parameters, operating frequency and fractional order. Therefore, a reasonable parameter setting and operating range of the frequency can greatly broaden the range of soft switching. Based on digital control, the driving frequency range can be limited to high-frequency band $[\omega_2, +\infty)$. Taking into account the working range and device withstand voltage, C_f and α_1 are set to 9.76 nF and 1.015, respectively. The corresponding critical coupling strength k_c is 0.073.

The ZVS conditions of leading leg (S_1 and S_2) and lagging leg (S_3 and S_4) will be analyzed in detail. Fig. 12(a) shows the voltage $V_{\rm DS}$ and current $I_{\rm DS}$ of S_1 and S_4 in the full range of test conditions. It shows that the leading leg is easier to realize ZVS than the lagging leg. Therefore, the lagging leg is the key to analyzing ZVS. The voltage lead phase γ of lagging leg is given in Fig. 12(b) and the blue line indicates the boundary where $\gamma = 0$. The voltage lead phase γ can be expressed as $\gamma = \varphi_p - \theta - \Delta t_h$, where the hardware delay time Δt_h includes the delay of MOSFET and is measured to be approximately 36 ns. In order to realize ZVS of lagging leg, S_3 and S_4 must be turned ON after the anti-parallel diode is turned ON. Thus, the condition for all switches to achieve ZVS is $\gamma \geq 0$. The operation waveforms are shown

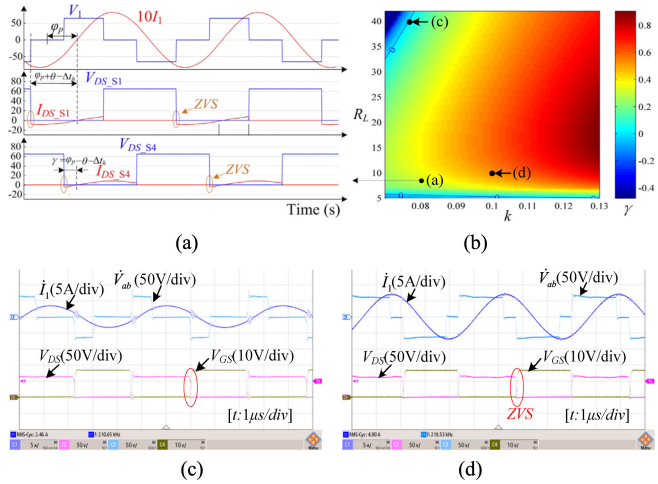

Fig. 12. Soft-switching analysis. (a) Voltage and current waveforms of the MOSFET. (b) Calculated leading phase γ as a function of the coupling strength k and load R_L. (c)–(d) Operation waveforms of the FOWPT system.

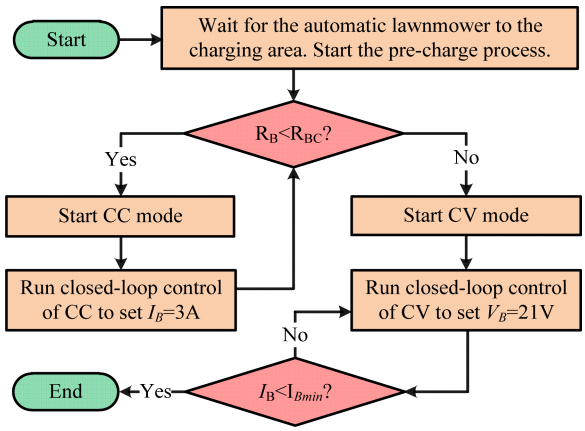

Fig. 13. Flowchart of CC and CV charging mode.

in Fig. 12(c) and (d), where $V_{\rm DS}$ and $V_{\rm GS}$ are the drain-source voltage and gate-source voltage of the switch. It demonstrates that the FOWPT system is designed to operate under the ZVS condition when $\gamma \geq 0$. The analysis of the switching tubes S_2 and S_3 is the same as that of S_1 and S_4 due to the symmetrical mode. Moreover, the loss of the inverter mainly includes conduction loss and switching loss of MOSFET. The conduction loss can be decreased by using a MOSFET with small ON-state resistance. In addition to designing soft switching, selecting a MOSFET with small rise and fall times can also be selected to reduce switching loss.

C. Experiment

This section will take an automatic lawnmower as an example to verify the feasibility of FOWPT. The flow chart of CC and CV charging mode is shown in Fig. 13. When the system starts to work, the PLL in Fig. 10(a) will be activated to maintain a constant fractional order. After the automatic lawnmower enters the charging region, the system will start the precharging process

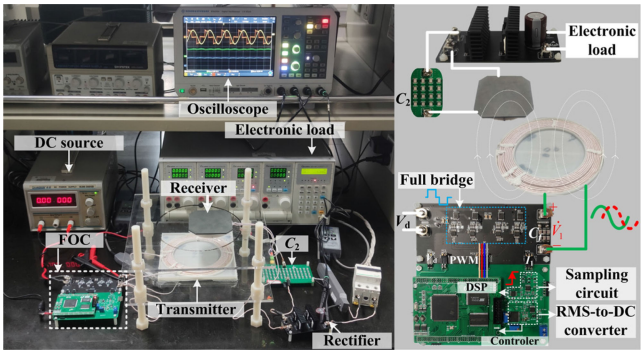

Fig. 14. Experimental prototype of the FOWPT system.

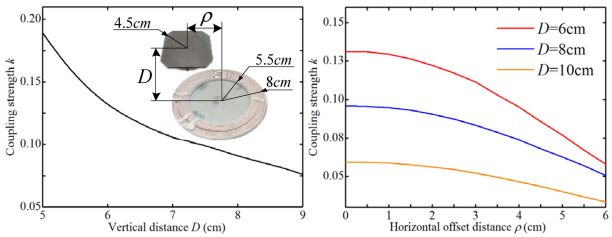

Fig. 15. Coupling strength k as a function of vertical distance D and horizontal offset distance ρ.

and outputs 0.3A current. Generally, the equivalent resistance R_B of the battery changes from time to time in the process of continuous charging. As we know, $R_{BC} = V_{\mathrm{Bref}}/I_{\mathrm{Bref}}$ is the critical equivalent resistance of the battery from CC mode to CV mode. According to (12) and (16), the equivalent resistance R_B can be obtained in real time. If $R_B < R_{BC}$, the closed-loop control of CC mode will be activated to set $I_B = 3$A. If $R_B \geq R_{BC}$, the system will directly run the closed-loop control of CV mode and output a CV ($V_B = 21$ V). In CV mode, the charging process will end, when the charging current is less than the cutoff current $I_{B\min} = 0.5$ A.

According to the above analysis and design, an FOWPT system for an automatic lawnmower is designed, and the experimental prototype is shown in Fig. 14. SI7172DP is adopted as a full-bridge converter. The model of the diode in the rectifier is STF20100. In the control circuit, DSP TMS320F28377D is used as a controller. The coils are fabricated by using Φ0.05 mm × 1000 silk-covered wire. The parameters of the experimental prototype are shown in Table I. The coupling strength k of coils as a function of vertical distance D and horizontal offset distance ρ is shown in Fig. 15.

Fig. 16 shows the steady-state characteristics of the FOWPT system with different positions and loads. In CC mode, the output current I_{B} remains constant after misalignment, as shown in Fig. 16(a) and (b). Benefiting from the frequency characteristics of FOWPT in (11) and the control strategy proposed in Fig. 9, the operating frequency of FOWPT system changes from 210.97 to 208.33 kHz. Meanwhile, the output current I_1 of the FOC changes from 5.09 to 5.03 A, according to the control block diagram in Fig. 11. It can be seen that the change of I_1 is very

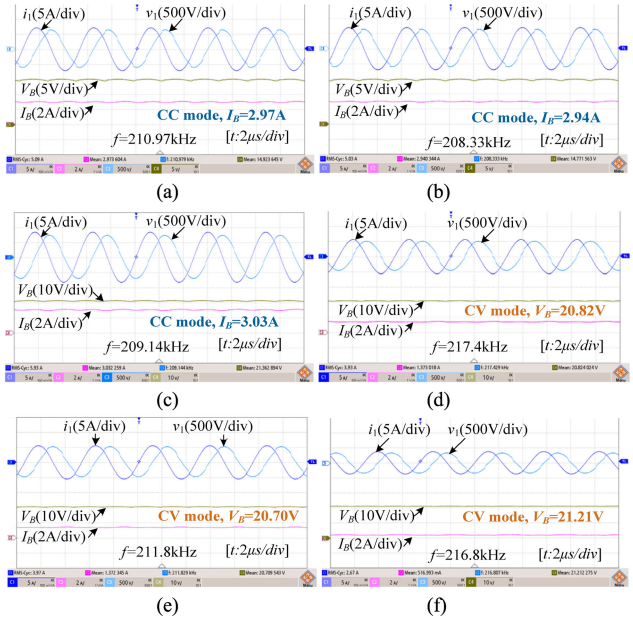

Fig. 16. Experimental waveforms during the CC and CV charging. (a) $D = 8$ cm, $\rho = 0$ cm, $R_B = 5\ \Omega$. (b) $D = 8$ cm, $\rho = 4$ cm, $R_B = 5\ \Omega$. (c) $D = 8$ cm, $\rho = 4$ cm, $R_B = 7\ \Omega$. (d) $D = 8$ cm, $\rho = 0$ cm, $R_B = 15\ \Omega$. (e) $D = 8$ cm, $\rho = 4$ cm, $R_B = 15\ \Omega$. (f) $D = 6$ cm, $\rho = 4$ cm, $R_B = 40\ \Omega$.

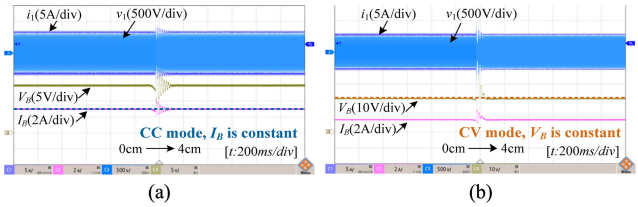

Fig. 17. Dynamic process when horizontal offset distance ρ varies rapidly from 0 to 4 cm: (a) in CC mode when $D = 8$ cm and $R_B = 5\ \Omega$; and (b) in CV mode when $D = 8$ cm and $R_B = 15\ \Omega$.

small, which is in good agreement with Fig. 6. It is the adjustment of the FOC in the transmitter that enables the system to operate in CC mode. Similarly, in CV mode, the output voltage V_B can also remain constant after misalignment, as shown in Fig. 16(d) and (e). When the automatic lawnmower is misalignment, the charging current and charging voltage can be maintained at I_{ref} and V_{ref}, respectively. It shows that the receiver can be charged steadily during the charging process, which meets the charging requirements of Li-ion battery.

In order to test the robust performance of the FOWPT system when the receiver moves, the dynamic process when horizontal offset distance ρ varies rapidly from 0 to 4 cm is shown in Fig. 17. It can be found that constant I_B in the CC mode and constant V_B in the CV mode can be maintained. In addition, Fig. 18 shows the output characteristics when vertical and horizontal distance changes, respectively. The proposed implementation method of FOC based on the phase-shift control enables the operating frequency ω to change in real time with distance. Meanwhile, the control block diagram in Fig. 11 will dynamically adjust the current of FOC to improve output accuracy. The current I_1

TABLE II
COMPARISONS WITH PREVIOUS WORKS

Reference	[10]	[12]	[14]	[13]	[27]	[25]	**This work**
Frequency	85kHz	500kHz	85kHz	85kHz	470~530kHz	50kHz	**200~224.5kHz**
Compensation network	LCC-LCC	S-S-S/S-P-S	LCC-LCC	Series-hybrid	S-S	S-S	**S-S**
Total number of capacitors and inductors	8	8	8	10	4	6	**4**
Transmitter coil	65×50cm	15cm	19.5cm	77.5×39.1cm	60cm	26cm	**16cm**
Receiver coil	32cm	15cm	19.5cm	77.5×39.1cm	60cm	26cm	**9cm**
Vertical misalignment tolerance	0% | 46.9%	0% | 13.3%	0% | 30.8%	25.4% | 18.2%	63.3% | 33.3%	0% | 11.5%	**22.2% | 66.7%**
Horizontal misalignment tolerance	0%	0%	0%	40.9%	/	0%	**44.4%**
Wireless communication	No	No	Yes	No	No	No	**No**
Additional DC-DC	No	No	No	No	No	No	**No**
Soft switch	Yes	Yes	Yes	Yes	No	No	**Yes**
Control complexity[a]	Asymmetric Tuning[(2)]	Switching topology[(1)]	Wireless communication[(2)]	Hybrid compensation[(1)]	Fractional method[(5)]	Fractional method[(4)]	**Fractional method[(3)]**
CC/CV mode	CC	CC/CV	No	No	No	CC	**CC/CV**
Output power	1.1~6.6kW	Max 172.8W	300W	3.3kW	100W	19.4~96.8W	**10.5~63W**
Transfer efficiency	/	/	~90.1%	/	~90%	85.7~91.6%	**87.9~92.7%**
DC-DC efficiency	72.3~92.4%	78~92.25%	/	~94%	/	/	**69.2~82.4%**

[a]The superscripts (1)–(5) represent the complexity, and the complexity increases as the number increases.

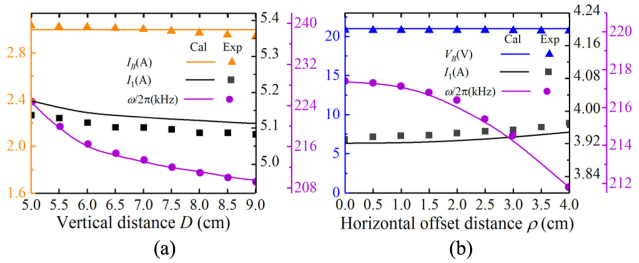

Fig. 18. Charging current I_B, voltage V_B, current I_1, and operating frequency $\omega/2\pi$ when the vertical distance D and horizontal offset distance ρ change. (a) $D\in[5, 9]$ and $\rho = 0$ cm when $R_B = 5\ \Omega$. (b) $\rho\in[0, 4]$ and $D = 8$ cm when $R_B = 15\ \Omega$.

basically remains unchanged, which implies that this system is insensitive to transfer distance. When the automatic lawnmower moves during the charging process, the primary-side controller can ensure a constant output with fine-tuning or even without adjustment. This is one of the advantages. The proposed FOWPT system provides the possibility for the AGV to move in a wide range during the wireless charging process.

Using the electronic load, the robustness of the proposed FOWPT system under step changes of R_B is investigated in CC and CV mode. As shown in Fig. 19(a)–(c), the system can quickly adjust to a stable state when R_B changes. The CC I_B in CC mode and CV V_B in CV mode can be realized only by controlling FOC. The proposed system not only realizes misalignment-tolerant charging, but also avoids complex and bulky receivers. Fig. 20 gives the circuit I_1 and voltage V_1 of FOC, the charging current I_B, the charging voltage V_B, and the transfer efficiency η in the charging process. The experimental results are in good agreement with the theory. It can be found that the output current is within $\pm 3\%$ in CC mode and the output voltage within $\pm 2\%$ in CV mode. The maximum transfer efficiency η is 92.7%, and the corresponding dc–dc (i.e., V_d to V_B) efficiency η_D is 82.4%.

Table II lists the comparison among different works. Vertical misalignment tolerance is described in the form of $\Delta D \mid D_0$, where ΔD is defined as the ratio of the vertical misalignment to the side length of the receiver; and D_0 is defined as the ratio of the initial vertical distance to the side length of the receiver. It should be noted that the side length of the receiver can be replaced by the square root of the length and width in the case of rectangular coils. Horizontal misalignment tolerance is expressed as $\Delta\rho$, which is defined as the ratio of the horizontal misalignment to the length of the receiver in the misalignment direction.

The coils in [12] and [13] are specially designed. Compared to the specially designed coils, the coil design of the proposed system is easier. Benefiting from high-order compensation topologies [10], [12]–[14], the control complexity is greatly reduced. Using the strategy of switching topology, the system in [12] achieves CC and CV modes, but the misalignment will lead to the fluctuation of output power. The series-hybrid compensation topology in [13] greatly improves misalignment tolerance. However, it is not suitable for compact and lightweight receivers.

Besides, the system in [25] not only requires two inverters, but also only realizes CC mode at a fixed transfer distance. The approximate modeling and low-precision fractional-order control strategy in [27] cannot maintain CC and CV modes. In addition, the control strategy of fractional-order elements is very complex in [25] and [27], which cannot guarantee the output accuracy under different loads and transfer distances. Based on this view, the proposed system achieves CC and CV modes with misalignment tolerance and meets the requirements of compact and lightweight receivers. The precise model and innovative implementation method based on the phase-shift control guarantee the accuracy of the output. Therefore, the proposed system is a suitable wireless charging solution for AGV.

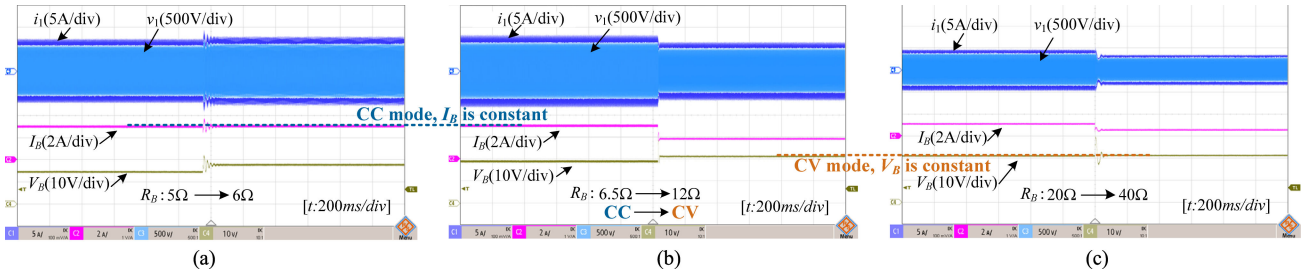

Fig. 19. Dynamic process of the proposed FOWPT system when $D = 8$ cm and $\rho = 0$ cm: (a) in CC mode when R_B changes from 5 to 6 Ω; (b) in CC to CV mode switching process when R_B changes from 6.5 to 12 Ω; and (c) in CV mode when R_B changes from 20 to 40 Ω.

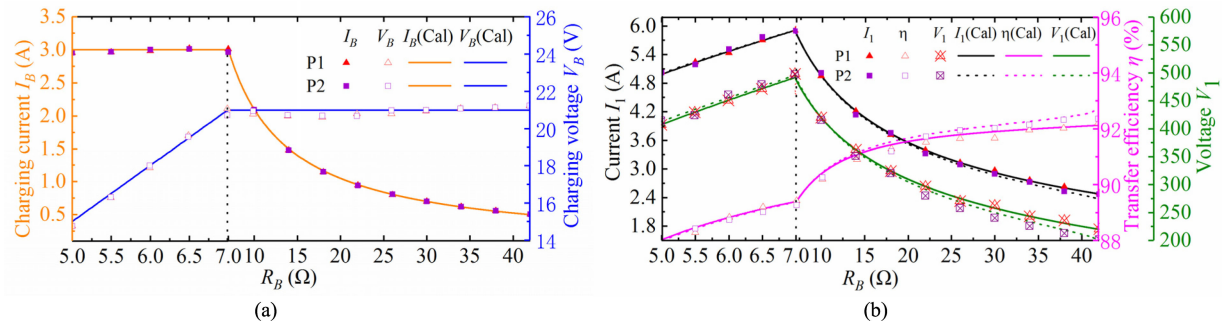

Fig. 20. Experimental results when the resistance R_B changes. (a) Charging current I_B and voltage V_B. (b) Current I_1, voltage V_1, and transfer efficiency η. P1: $D = 8$ cm and $\rho = 0$ cm; P2: $D = 8$ cm and $\rho = 4$ cm.

V. Conclusion

This article proposed a misalignment-tolerant FOWPT system for CC and CV charging. According to the principle of fractional-order autonomous circuit, the circuit model of the system was established. The theoretical and experimental results showed that the natural resonant frequency and operating frequency can be adjusted adaptively with the change of transfer distance and load. Compared with the conventional IPT system, the proposed system was able to maintain stable output under the misalignment of coupling coils. The 63-W experimental prototype of the automatic lawnmower was built. The horizontal misalignment tolerance was within 44.4%. Meanwhile, the vertical misalignment tolerance was within 22.2% at the initial position $D = 6$ cm. Based on the frequency characteristics and the new implementation method of FOWPT, the prototype can maintain the output current within ±3% in CC mode and the output voltage within ±2% in CV mode. Therefore, the system has strong misalignment tolerance, light receiver weight, and high design freedom, which provides a new wireless charging solution for AGV. In the future article, we will focus on concise modeling and implementation methods of FOWPT, and exploring the physical mechanism and valuable characteristics of fractional-order circuits.

References

[1] L. Li, H. Liu, H. Zhang, and W. Xue, "Efficient wireless power transfer system integrating with metasurface for biological applications," *IEEE Trans. Ind. Electron.*, vol. 65, no. 4, pp. 3230–3239, Apr. 2018.

[2] Z. Yan, B. Song, Y. Zhang, K. Zhang, Z. Mao, and Y. Hu, "A rotation-free wireless power transfer system with stable output power and efficiency for autonomous underwater vehicles," *IEEE Trans. Power Electron.*, vol. 34, no. 5, pp. 4005–4008, May 2019.

[3] Y. Guo, L. Wang, Y. Zhang, S. Li, and C. Liao, "Rectifier load analysis for electric vehicle wireless charging system," *IEEE Trans. Ind. Electron.*, vol. 65, no. 9, pp. 6970–6982, Sep. 2018.

[4] J. Mai, Y. Wang, Y. Yao, and D. Xu, "Analysis and design of high-misalignment-tolerant compensation topologies with constant-current or constant-voltage output for IPT systems," *IEEE Trans. Power Electron.*, vol. 36, no. 3, pp. 2685–2695, Mar. 2021.

[5] R. Yue, C. Wang, H. Li, and Y. Liu, "Constant-voltage and constant-current output using P-CLCL compensation circuit for single-switch inductive power transfer," *IEEE Trans. Power Electron.*, vol. 36, no. 5, pp. 5181–5190, May 2021.

[6] M. G. S. Pearce, G. A. Covic, and J. T. Boys, "Robust ferrite-less doubled topology for roadway IPT applications," *IEEE Trans. Power Electron.*, vol. 34, no. 7, pp. 6062–6075, Jul. 2019.

[7] S. Kim, G. A. Covic, and J. T. Boys, "Tripolar pad for inductive power transfer systems for EV charging," *IEEE Trans. Power Electron.*, vol. 32, no. 7, pp. 5045–5057, Jul. 2017.

[8] E. S. Lee, Y. H. Sohn, B. G. Choi, S. H. Han, and C. T. Rim, "A modularized IPT with magnetic shielding for a wide-range ubiquitous WI-power zone," *IEEE Trans. Power Electron.*, vol. 33, no. 11, pp. 9669–9690, Nov. 2018.

[9] W. Tang, Q. Zhu, J. Yang, D. Song, M. Su, and R. Zou, "Simultaneous 3-D wireless power transfer to multiple moving devices with different power demands," *IEEE Trans. Power Electron.*, vol. 35, no. 5, pp. 4533–4546, May 2020.

[10] Y. Chen, H. Zhang, C.-S. Shin, C.-H. Jo, S.-J. Park, and D.-H. Kim, "An efficiency optimization-based asymmetric tuning method of double-sided *LCC* compensated WPT system for electric vehicles," *IEEE Trans. Power Electron.*, vol. 35, no. 11, pp. 11475–11487, Nov. 2020.

[11] K. Song, Z. Li, J. Jiang, and C. Zhu, "Constant current/voltage charging operation for series–series and series–parallel compensated wireless power transfer systems employing primary-side controller," *IEEE Trans. Power Electron.*, vol. 33, no. 9, pp. 8065–8080, Sep. 2018.

[12] Y. Li *et al.*, "Reconfigurable intermediate resonant circuit based WPT system with load-independent constant output current and voltage for charging battery," *IEEE Trans. Power Electron.*, vol. 34, no. 3, pp. 1988–1992, Mar. 2019.
[13] L. Zhao, D. J. Thrimawithana, U. K. Madawala, A. P. Hu, and C. C. Mi, "A misalignment-tolerant series-hybrid wireless EV charging system with integrated magnetics," *IEEE Trans. Power Electron.*, vol. 34, no. 2, pp. 1276–1285, Feb. 2019.
[14] Y. Yao, H. Cheng, Y. Wang, J. Mai, K. Lu, and D. Xu, "An FDM-based simultaneous wireless power and data transfer system functioning with high-rate full-duplex communication," *IEEE Trans. Ind. Inform.*, vol. 16, no. 10, pp. 6370–6381, Oct. 2020.
[15] J. Yin, D. Lin, C. K. Lee, T. Parisini, and S. Y. Hui, "Front-end monitoring of multiple loads in wireless power transfer systems without wireless communication systems," *IEEE Trans. Power Electron.*, vol. 31, no. 3, pp. 2510–2517, Mar. 2016.
[16] Y. Guo, Y. Zhang, S. Li, C. Tao, and L. Wang, "Load parameter joint identification of wireless power transfer system based on the DC input current and phase-shift angle," *IEEE Trans. Power Electron.*, vol. 35, no. 10, pp. 10542–10553, Oct. 2020.
[17] S. Assawaworrarit, X. Yu, and S. Fan, "Robust wireless power transfer using a nonlinear parity-time-symmetric circuit," *Nature*, vol. 546, no. 7658, pp. 387–390, Jun. 2017.
[18] J. A. Tenreiro Machado and A. M. S. F. Galhano, "Fractional order inductive phenomena based on the skin effect," *Nonlinear Dyn.*, vol. 68, no. 1, pp. 107–115, 2012.
[19] B. Ross, "The development of fractional calculus 1695–1900," *Historia Mathematica*, vol. 4, no. 1, pp. 75–89, Apr. 1977.
[20] A. A. Kilbas, H. M. Srivastava, and J. J. Trujillo, *Theory and Applications of Fractional Differential Equations*. Amsterdam, The Netherlands: Elsevier, 2006.
[21] I. Podlubny, *Fractional Differential Equations.* New York, NY, USA: Academic Press, 1999.
[22] A. G. Radwan and K. N. Salama, "Passive and active elements using fractional $L_\beta C_\alpha$ circuit," *IEEE Trans. Circuits Syst. I, Regular Papers*, vol. 58, no. 10, pp. 2388–2397, Oct. 2011.
[23] B. Zhang, R. H. Huang, and D. Y. Qiu, "Fractional order series resonance system for wireless electric energy transmission," U.S. Patent 9620965, 2017.
[24] Y. Jiang and B. Zhang, "High-power fractional-order capacitor with $1 < \alpha < 2$ based on power converter," *IEEE Trans. Ind. Electron.*, vol. 65, no. 4, pp. 3157–3164, Apr. 2018.
[25] Y. Jiang, B. Zhang, and J. Zhou, "A fractional-order resonant wireless power transfer system with inherently constant current output," *IEEE Access*, vol. 8, pp. 23317–23323, 2020.
[26] C. Rong, B. Zhang, and Y. Jiang, "Analysis of a fractional-order wireless power transfer system," *IEEE Trans. Circuits Syst. II, Exp. Briefs*, vol. 67, no. 10, pp. 1755–1759, Oct. 2020.
[27] Y. Jiang and B. Zhang, "A fractional-order wireless power transfer system insensitive to resonant frequency," *IEEE Trans. Power Electron.*, vol. 35, no. 5, pp. 5496–5505, May 2020.
[28] X. Chen, Y. Chen, B. Zhang, and D. Qiu, "A modeling and analysis method for fractional-order DC–DC converters," *IEEE Trans. Power Electron.*, vol. 32, no. 9, pp. 7034–7044, Sep. 2017.
[29] A. U. Hassan, H. Hodaei, M. A. Miri, M. Khajavikhan, and D. N. Christodoulides, "Nonlinear reversal of the PT-symmetric phase transition in a system of coupled semiconductor micro-ring resonators," *Phys. Rev. A*, vol. 92, no. 6, Dec. 2015, Art. no. 063807.
[30] M. Sivarama Krishna, S. Das, K. Biswas, and B. Goswami, "Fabrication of a fractional order capacitor with desired specifications: A study on process identification and characterization," *IEEE Trans. Electron. Devices*, vol. 58, no. 11, pp. 4067–4073, Nov. 2011.
[31] H. Samavati, A. Hajimiri, A. R. Shahani, G. N. Nasserbakht, and T. H. Lee, "Fractal capacitors," *IEEE J. Solid-State Circuits*, vol. 33, no. 12, pp. 2035–2041, Dec. 1998.
[32] M. C. Tripathy, D. Mondal, K. Biswas, and S. Sen, "Experimental studies on realization of fractional inductors and fractional-order bandpass filters," *Int. J. Circuit Theory Appl.*, vol. 43, no. 9, pp. 1183–1196, Jan. 2015.

Chao Rong was born in Shanxi, China, in 1995. He received the B.S. degree in electrical engineering and automation from the South China University of Technology, Guangzhou, China, in 2018, where he is currently working toward the Ph.D. degree in power electronics and power drives.

His research interests include wireless power transfer technology and fractional-order system.

Bo Zhang (Senior Member, IEEE) was born in Shanghai, China, in 1962. He received the B.S. degree in electrical engineering from Zhejiang University, Hangzhou, China, in 1982, the M.S. degree in power electronics from Southwest Jiaotong University, Chengdu, China, in 1988, and the Ph.D. degree in power electronics from the Nanjing University of Aeronautics and Astronautics, Nanjing, China, in 1994.

He is currently a Professor with the School of Electric Power, South China University of Technology, Guangzhou, China. He has authored or coauthored more than 450 papers and held 102 patents. He has authored eight monographs. His research interests include nonlinear analysis, modeling, and control of power electronic converters, and wireless power transfer applications.

Yanwei Jiang received the B.S. degree in electrical engineering and the M.S. degree in control theory and control engineering from Fuzhou University, Fuzhou, China, in 2012 and 2015, respectively, and the Ph.D. degree in power electronics from the School of Electric Power, South China University of Technology, Guangzhou, China, in 2019.

He is currently a lecturer with Fuzhou University, Fuzhou, China. His research interests include wireless power transfer applications, control of power electronics, and fractional-order system.

Xujian Shu received the B.S. degree in electrical engineering and automation from the China University of Mining and Technology, Xuzhou, China, in 2015. She is currently working toward the Ph.D. degree in power electronics at the School of Electric Power, South China University of Technology, Guangzhou, China.

Her research interests include wireless power transfer applications, power electronics converters, and fractional-order system.

Zhihao Wei was born in Shandong, China, in 1990. He received the B.S. and M.S. degrees in electrical engineering from Qingdao University, Qingdao, China, in 2015 and 2018, respectively. He is currently working toward the Ph.D. degree in power electronics and power drives at the School of Electric Power, South China University of Technology, Guangzhou, China.

His research interests include wireless power transfer technology and fractional-order system.